Journal of Alloys and Compounds 505 (2010) 113–117

Contents lists available at ScienceDirect

Journal of Alloys and Compounds

journal homepage: www.elsevier.com/locate/jallcom

Effect of rapid solidification on mechanical properties of a lead free Sn–3.5Ag solder

R.M. Shalaby*

Metal Physics Lab., Physics Department, Faculty of Science, Mansoura University, Mansoura 35516, Egypt

ARTICLE INFO

Article history:
Received 19 March 2010
Received in revised form 13 May 2010
Accepted 22 May 2010
Available online 19 June 2010

Keywords:
Lead free solder
Rapid solidification
Mechanical properties
Tensile properties
Melting point

ABSTRACT

The melt-spinning processes of Sn–3.5Ag, Sn–3.5Ag–2In, Sn–3.5Ag–2Bi and Sn–3.5Ag–2Zn lead free solders were investigated and analyzed. The results showed that formation of intermetallic compounds of ε-Ag_3Sn, $In_{0.2}Sn_{0.8}$ and AgZn embedded in Sn matrix phase, were produced during melt-spinning technique not found under equilibrium conditions. Addition of small amount (2 wt.%) In, Bi, or Zn refines the grain size, increases H_v, delay the fracture strength and improves creep resistance. The ternary alloys exhibits mechanical properties superior to that of the binary alloy Sn–3.5Ag because it has a uniform fine dispersion of precipitates and small effective grain size. It is found that in the lead free solder has composition of Sn–3.5Ag–2In, Sn–3.5Ag–2Bi and Sn–3.5Ag–2Zn melt-spun alloys, have eutectic composition which could be attributed to the shift of eutectic point under rapid solidification. The addition of indium, bismuth and zinc to the Sn–Ag binary system lowers the melting temperature.

1. Introduction

In recent years, many lead free solder alloys begin to replace the Pb-containing solder alloys in microelectronic industry and come into use in some packaging processes and interconnects of certain microelectronic components. The elimination of Pb-containing in consumer microelectronic products has been common understood in the world. Lead free solder Sn–3.5Ag was considered as one of candidates which could replace Pb-containing solder in microelectronic packaging and interconnects. Though tin–lead (Sn–Pb) solders fulfill most soldering requirements in electronics manufacturing, alternative solders are needed to meet more stringent environmental regulations, requirements for greater mechanical reliability, and more demanding high temperature service environments such as under the-hood in automobiles and in avionics systems [1–4]. The tin–silver eutectic alloy (3.5%) is an especially attractive candidate to meet these requirements. It is free of toxic lead (Pb), offers better mechanical properties, [5] is better for high temperature application due to its higher melting temperature, and has good wetting behavior on copper and copper alloys [6]. Acceptable Pb-free solder must satisfy both, the process requirements and the reliability issues. The new solders must form joints with acceptable strength, and, at the same time, must withstand thermal fatigue over the projected operational life of the assembly. Mechanical properties and microstructure are, therefore, among the main parameters to be controlled in the candidate solders in an industrial process. A creep process and microstructure for a lead free solder Sn–Ag has been studied [7]. Many studies of lead free solders and soldering have been performed. Most of them have focused on Sn-based alloys. In particular, Sn–Ag alloys are expected to be a substitute for the Sn–Pb eutectic solder, because they have better mechanical properties (ductility, creep resistance and thermal resistance) than Sn–Pb solder [8]. Thus, the Sn–Ag alloy system was applied as the first lead free solder in the world [9], although the melting temperature is higher and the wetting is poorer than conventional Sn–Pb eutectic solder. Microstructures of eutectic Sn–3.7 wt.%Ag–0.9 wt.%Zn solder were investigated under different cooling rates (0.16 K/s, about 10^2 K/s and about 10^4 K/s) [10]. The effect of the addition of In, up to 1 wt.% on the formation of intermetallic compounds in the solidified Sn–3.7%Ag–0.9%Zn lead free solder was investigated [11]. Effect of rapid solidification and cooling rates on microstructure and microhardness of lead free Sn–3.5Ag solder has been studied [12,13]. The mechanical properties of some promising Sn–3.5Ag based lead free solders, such as hardness and Young's modulus, were explored by instrumented nano-indentation [14]. It was found that the hardness was dependent on the loading rate. The tensile properties of Sn–3.5Ag, Sn–03.5Ag–0.75Cu and Sn–3.5Ag–2Bi lead free solders were investigated and compared with those of a Sn–Pb eutectic solder [15]. The microstructure of a solidifying lead free Sn–3.5Ag solder alloy is found to be highly sensitive to the surface condition of the copper substrate [16]. Therefore, In, Bi and Zn were chosen in the present work as alloying element to Sn–3.5Ag alloy in order to improve the soldering property in electronic packaging by lowering melting

* Tel.: +002 050 2242388; fax: +002 0502246781.
E-mail address: rizk1969@yahoo.co.uk.

0925-8388/$ – see front matter © 2010 Elsevier B.V. All rights reserved.
doi:10.1016/j.jallcom.2010.05.179

point. Also, rapid solidification was chosen as a preparing technique for the alloys. It is an important non-equilibrium processing technique and has been frequently employed to improve the properties and performance of existing alloys and also for the development of entirely new compositions. It involves cooling of metallic melts at rates > 10^4 K/s and results in significant microstructural and constitutional changes. The aim of the present work is to study the effects of rapid solidification and alloying ternary elements on the structure, melting behavior, creep resistance, mechanical properties and tensile properties of Sn–3.5Ag lead free solder.

2. Experimental procedures

Four alloys of compositions Sn–3.5 wt.%Ag, Sn–3.5 wt.%Ag–2.0 wt.%In, Sn–3.5 wt.%Ag–2.0 wt.%Bi and Sn–3.5 wt.%Ag–2.0 wt.%Zn have been produced by a single copper roller melt-spinning technique. Required quantities of the used metals were weighed out and melted in a porcelain crucible. After the alloys were molten, the melt was thoroughly agitated to effect homogenization. The casting was done in air at a melt temperature of 600 °C. The speed of the copper wheel was fixed at 2900 rpm; which corresponds to a linear speed of 30.4 m/s. X-ray diffraction (XRD) analysis is carried out with a X-ray diffractometer (XRD, X'pert PRO, PANalytical using CuKα target with secondary monochromator, in Central Metallurgical R and D Institute, Technical Service Department, El-Tebbin, Helwan, Cairo) was used to identify the structure of all produced alloys. The melting temperature of these alloys was determined by differential scanning calorimetry [(DSC-16, Setaram, France) in Technical Service Department, El-Tebbin, Helwan, Cairo] with a heating rate 10 K/min. The internal friction and dynamic young's modulus of melt-spun alloys was examined by a dynamic resonance method. The Vickers microhardness number (H_v) is measured using the FM-7 microhardness tester. More than 15 indents, to each value were made on each sample to reveal any hardness variation due to the presence of more phases, with one phase soft, ductile and another phase considerably harder.

3. Results and discussions

3.1. Structure

The XRD diffraction patterns for the as-quenched Sn–3.5Ag, Sn–3.5Ag–2In, Sn–3.5Ag–2Bi and Sn–3.5Ag–2Zn melt-spun alloys are shown in Fig. 1. For Sn–3.5Ag is shown in Fig. 1(a) contains pure β-Sn phase, and ε-Ag_3Sn intermetallic compound phases embedded in the Sn matrix. For Sn–3.5Ag–2In alloy Fig. 1(b), the number of peaks of the ε-Ag_3Sn, intermetallic compound phase as the same while the results indicates the formation new intermetallic compounds $Ag_{0.8}Sn_{0.2}$ and $In_{0.2}Sn_{0.8}$ phases. For Sn–3.5Ag–2Bi alloy Fig. 1(c), the number of peaks and intensity due to ε-Ag_3Sn increases. For Sn–3.5Ag–2Zn, Fig. 1(d) causes the presence of new intermetallic compound AgZn in addition to the ε-Ag_3Sn, $Ag_{0.8}Sn_{0.2}$ and β-Sn phases. The intermetallic compounds AgZn has cubic crystal structure, space group *pm*-3*m* and lattice parameter 3.156 Å and Ag0.8Sn0.2 has hexagonal close-backed structure, space group *P*63/*mmc*, space group no. 194 and lattice parameter $a = b = 2.9658$ Å, $c = 4.784$ Å. The details of the XRD analysis are shown in Table 1.

Table 1 shows the variation of axial ratio *c*/*a* with different compositions. It is found that the axial ratio increases to maximum value about 0.54555 Å at 2 wt.%Zn. The average grain size for all compositions was estimated from the diffraction peaks by using the Scherrer equation [17]: $d = \lambda/B\cos\theta$, where λ is the X-ray wavelength, *B* is the full width at half maximum [FWHM] of the XRD peak and θ is the diffraction angle. The results show that the minimum value of particle size was observed for Sn–3.5Ag–2Zn melt-spun alloy is 180 nm. It was also found that the addition of small amount of In, Bi and Zn at level 2 wt.% to the eutectic Sn–3.5Ag alloy refines the effective grain size and retains the fine dispersion of Ag-rich precipitates in the β-Sn matrix through the solidification microstructure. Also the variations of the volume of the unit cell and the measured density have an opposite trend, in agreement

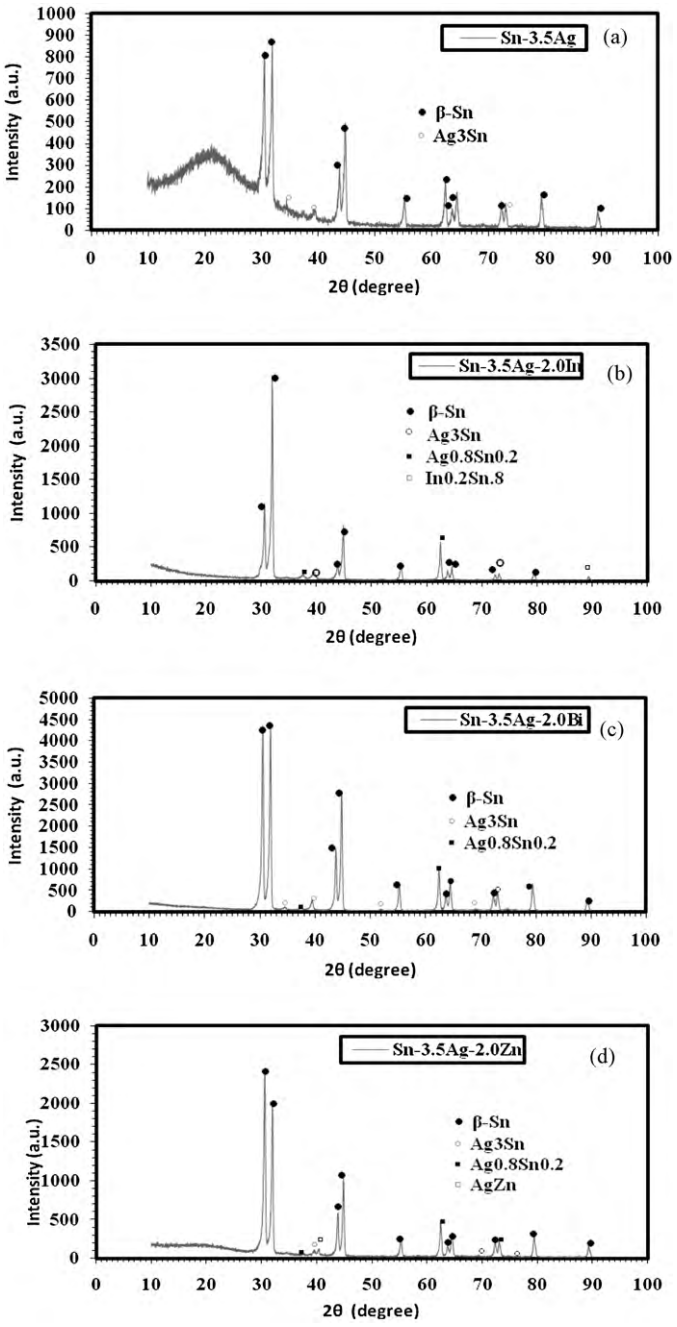

Fig. 1. The XRD patterns of as-quenched melt-spun alloys: (a) Sn–3.5Ag, (b) Sn–3.5Ag–2In, (c) Sn–3.5Ag–2Bi, and (d) Sn–3.5Ag–2Zn.

with the following equation [18]:

$$\sum A = \frac{\delta v}{1.6602}$$

where $\sum A$ is the sum of the atomic weight in the unit cell, δ is the measured density in g/cm^3 and v is the volume of the unit cell in nm^3. The value of the measured density for pure Sn rapidly solidified is 7 g/cm^3, when this value is substituted in above equation, it gives 456.5 for $\sum A$. By dividing the value of $\sum A$ by the atomic weight of Sn (118.69), it gives the number of atoms per unit cell 3.84, which must be 4 for β-Sn. Therefore, some of the atoms may be missing from a certain fraction of these lattice sites that they would be expected to occupy.

Table 1
The details of the XRD analysis.

Alloy	Phases	Crystal system	Crystal size (nm)	a (Å)	c (Å)	c/a
Sn–3.5Ag	β-Sn	Body centered tetragonal	325	5.84247	3.17804	0.54395
	Ag_3Sn	Orthorhombic	352			
Sn–3.5Ag–2In	β-Sn	Body centered tetragonal	290	5.83612	3.18013	0.5449
	Ag_3Sn	Orthorhombic	327			
	$Ag_{0.8}Sn_{0.2}$	Hexagonal	215			
	$In_{0.2}Sn_{0.8}$		369			
Sn–3.5Ag–2Bi	β-Sn	Body centered tetragonal	269	5.8457	3.1878	0.54532
	Ag_3Sn	Orthorhombic	207			
	$Ag_{0.8}Sn_{0.2}$	Hexagonal	205			
Sn–3.5Ag–2Zn	β-Sn	Body centered tetragonal	241	5.8457	3.1869	0.54544
	Ag_3Sn	Orthorhombic	180			
	$Ag_{0.8}Sn_{0.2}$	Hexagonal	203			
	AgZn	Cubic	228			

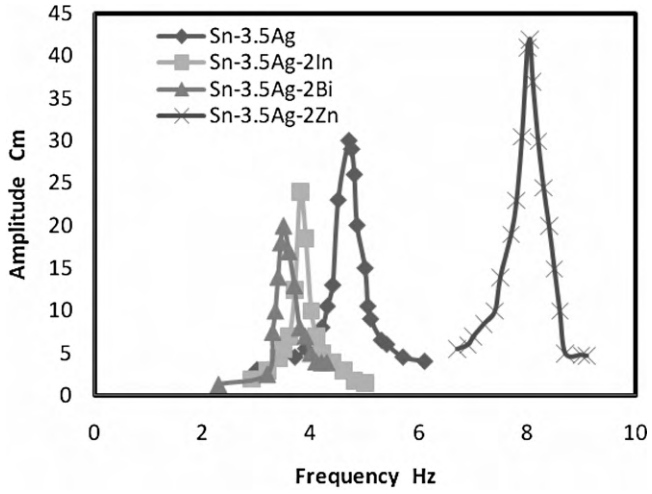

Fig. 2. Typical resonance curves of melt-spun alloys.

4. Mechanical properties

4.1. Internal friction and dynamic Young's modulus

Fig. 2 shows the resonance curves for melt-spun ribbons of Sn–3.5Ag–2X(X = In, Bi or Zn). The measured internal friction Q^{-1} values are listed in Table 2 as function of composition.

It is concluded that the internal friction is sensitive to the content of In, Bi and Zn as alloying elements to the binary Sn–3.5Ag as indicated in Table 2. It is shown that the internal friction Q^{-1} decreased with the addition of In, Bi and Zn is explained by a reduction in transformable shear stress with largest free volume. Generally it is found that the addition of In, Bi and Zn cause a marked decrease in friction at used cooling rate. Consequently, high damping capacity is practical engineering importance in limiting the amplitude of vibration at resonance conditions and thereby reducing the likelihood of fatigue failure. Table 2 shows the variation of the dynamic Young's modulus E with the variation of different compositions. At first the value of E for Sn–3.5Ag rapidly solidified was found to be 54 GPa. After the addition of In, Bi or Zn to Sn–3.5Ag, the value of E increases to a maximum value 64 GPa at level 2 wt.%Zn. This observed behavior of Young's modulus with composition can be explained in terms of the variation in the c/a ratio of the unit cell of Sn matrix. The increase in the c/a ratio means the stretching of the unit cell along the c-axis, this modification in the shape of the unit cell of the Sn matrix may result in an increase in the dynamic young's modulus. Also, it is due to the presence of hard intermetallic compounds which act as hard inclusions in the soft matrix. The calculated tensile fracture strength (σ_f), tensile fracture strain ($\varepsilon_{t,f} = \sigma_f/E$), compressive yield strain ($\varepsilon_{c,y} = H_v/3$) are shown in Table 3. It is found that the tensile fracture strength, compressive yield strength increasing with the addition of In, Bi or Zn. This may be due to high performance metal alloys are never single phase but generally consists of a matrix interspersed by areas of an intermetallic phases as Ag_3Sn, $Ag_{0.8}Sn_{0.2}$ and AgZn [19].

Table 2
Internal friction (Q^{-1}) values and dynamic Young's modulus of melt-spun alloys.

Alloy	Q^{-1}	E (GPa)
Sn–3.5Ag	0.072	54.3
Sn–3.5Ag–2In	0.063	55.5
Sn–3.5Ag–2Bi	0.052	58.6
Sn–3.5Ag–2Zn	0.041	64.2

4.2. Hardness indentation and micro-creep behavior

Resistance to plastic indentation was determined by an indentation hardness test, in which a small hard indenter is pressed into the surface by a standard load and the size of indentation produced by it is then measured. Fig. 3 shows the variation of microhardness H_v with applied load at dwell time 5 s. For Sn–3.5Ag, H_v has the lowest value 185.22 MPa. After addition the indium, bismuth and zinc at 2 wt.% level the H_v increases up to reach 415.52 MPa

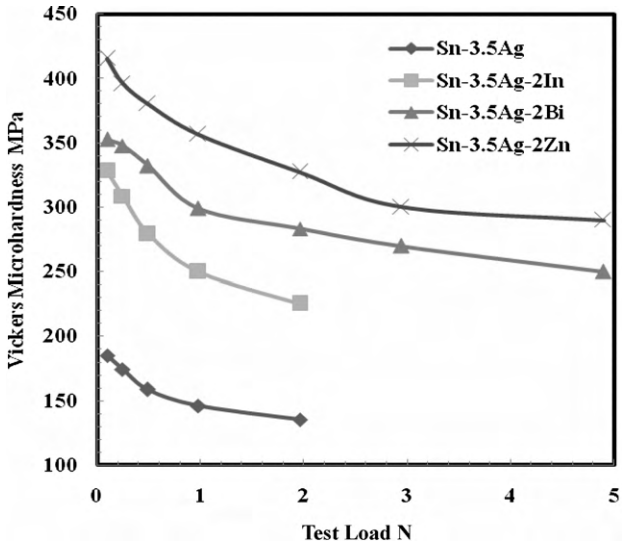

Fig. 3. The variation of H_v with test load.

Table 3
Vickers microhardness and calculated tensile properties of melt-spun alloys.

Alloy	H_v (MPa)	$\sigma_{c,y}$ (MPa)	σ_f (GPa)	$\varepsilon_{c,y}$ (10^{-3})	$\varepsilon_{t,f}$
Sn–3.5Ag	185.22	61.74	24	1.14	0.444
Sn–3.5Ag–2In	328.3	109.43	24.8	1.97	0.446
Sn–3.5Ag–2Bi	352.8	117.6	26.08	2	0.4458
Sn–3.5Ag–2Zn	415.52	138.50	28.58	2.15	0.4451

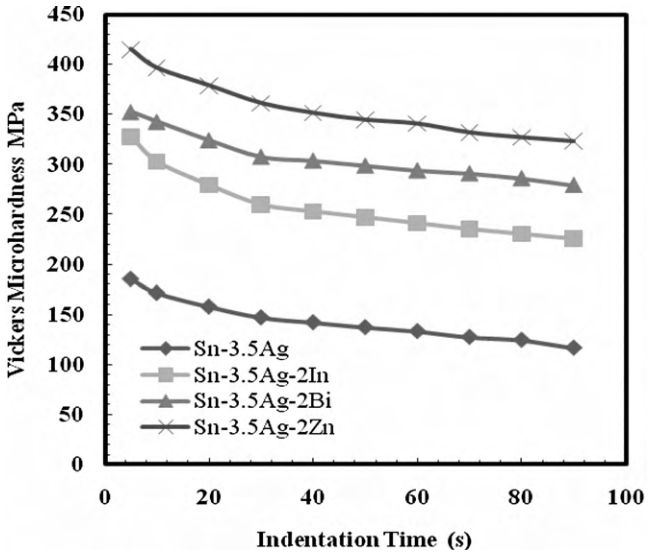

Fig. 4. Variation of H_v with dwell time.

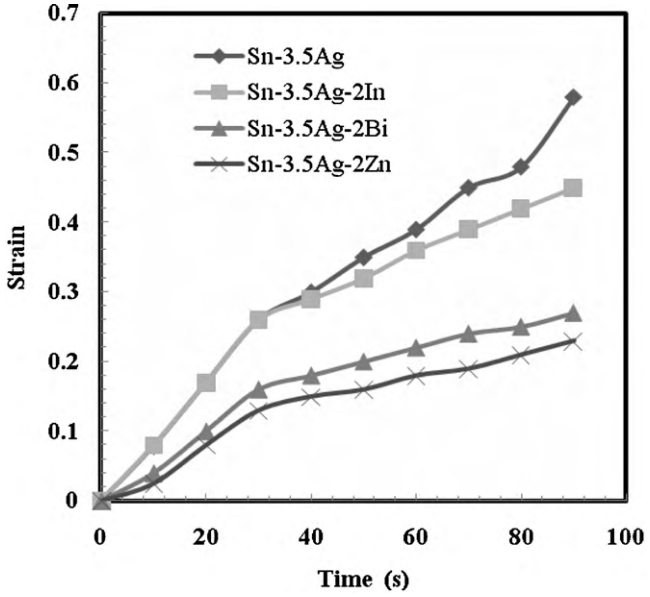

Fig. 5. The creep behavior of as-quenched melt-spun alloys.

at 2 wt.%Zn. This is attributed to the presence of more intermetallic compounds Ag_3Sn and AgZn and refinement the crystal size. Also, this behavior can be explained in terms of the alloy structure and resulting properties. Also, the relatively high amount of hard AgZn phase is likely present. The experimental determinations involve the measurement of the time and load dependence of hardness in addition to the effect of In, Bi and Zn content in the binary Sn–3.5Ag alloy. In Fig. 3 the fracture happens at 1.96 N and 5 s for Sn–3.5 Ag and Sn–3.5Ag–2In. After adding the Bi and Zn at 2 wt.% level the fracture is delayed up to 4.9 N and 5 s. This is attributed to the presence of more intermetallic compound Ag_3Sn, AgZn and refinement of grain size by effect of rapid solidification. The changes in microhardness H_v with indentation time and constant load 0.098 N up to point of fracture shown in Fig. 4. It is found in this work and others [20] that H_v decreases by increasing dwell time and since the hardness is given by $H_v = 0.102\,F/s$ MPa, where F is the test load (N) and s is the surface area of an indentation (mm^2) and in this case the test load is kept constant at 0.098 N. Therefore, the increase in area (strain) with the indentation time under constant load by definition is creep. The strain here is considered as the fractional change in area and is given by strain = $\Delta S/S$, %, where $\Delta S = S - S_o$, and S_o is considered to be the area at the minimum indentation time. The measurement of creep by this method is termed "micro-creep"; the term micro-creep comes from applying the stress to a very small area comparable to the area of a grain, and it is observed by microscope. Plotting the strain with indentation time, we obtain a typical creep curve, as shown in Fig. 5. Both Sn–3.5Ag, Sn–3.5Ag–2In, Sn–3.5Ag–2Bi and Sn–3.5Ag–2Zn alloys from 5 s to 90 s exhibit the primary creep stage; however the creep resistance of Sn–3.5Ag–2In, Sn–3.5Ag–2Bi, Sn–3.5Ag–2Zn are higher than that of Sn–3.5Ag due to generate fine structure in the solder as a result of rapid solidification. The high creep rate of as-quenched melt-spun alloy Sn–3.5Ag shown in Fig. 5 may be due to the high concentration of vacancies obtained by rapid solidification [21].

5. Thermal properties

The melting behavior of each of the Sn–3.5Ag–2X(X = In, Bi or Zn) rapidly solidified from melt during heating was investigated by differential scanning calorimetry (DSC) at a heating rate of 10 °C/min under an argon atmosphere. Fig. 6 shows the DSC endothermic peaks of Sn–3.5Ag–2X alloys during heating. There is only one endothermic peak corresponding to the melting reaction. For Sn–3.5Ag alloy the melting point is equal to 219 °C which decreases by 2 °C than that obtained by normal casting technique. This decrease can be attributed to the effect of rapid solidification which agrees with other works [22].

Table 4
Thermal analysis of melt-spun alloys.

Alloy	T_m	Solidus temperature (T_s) (°C)	Liquidus temperature (T_l) (°C)	Pasty range (°C)	Enthalpy (μv s/mg)
Sn–3.5Ag	219	219	219	0	2.613
Sn–3.5Ag–2In	212.1	212.1	212.1	0	16.57
Sn–3.5Ag–2Bi	214.5	214.5	214.5	0	19.3
Sn–3.5Ag–2Zn	216	216	216	0	17.78

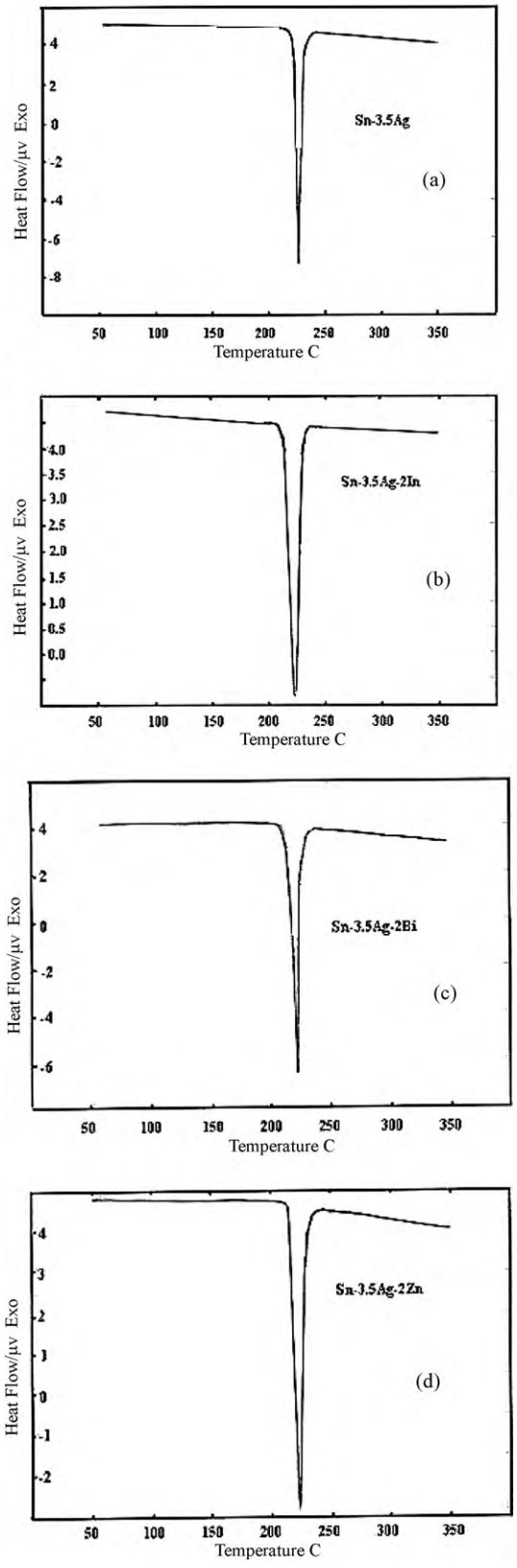

Fig. 6. The differential scanning calorimetry (DSC) of as-quenched melt-spun (a) Sn–3.5Ag (b) Sn–3.5Ag–2In (c) Sn–3.5Ag–2Bi and (d) Sn–3.5Ag–2Zn.

It is found that in the lead free solder has composition of Sn–3.5Ag–2In, Sn–3.5Ag–2Bi and Sn–3.5Ag–2Zn cooled with a high rate, has eutectic composition which could be attributed to the shift of eutectic point under rapid solidification. Also, the addition of ternary element In, Bi or Zn reduced the melting point of the eutectic Sn–3.5Ag alloy to 212 °C at 2 wt.%In. These decreases in melting point can be attributed to the dissolution or precipitation of In and Bi phases as a lower melting point phase than that of the eutectic matrix. Also, this reduction may be attributed the decrease of the crystalline size. From Fig. 6 the melting point (T_m), solidus temperature (T_s), liquidus temperature (T_l), enthalpy of fusion (ΔH_f) and pasty range of these alloys were calculated and presented in Table 4. The pasty range (solidus–liquidus distance) for the all eutectic alloys equal to zero. The pasty range property it is very important for electronic applications.

6. Conclusions

From previous studies it is concluded that:

Rapid solidification technology and small addition of In, Bi and Zn to Sn–3.5Ag eutectic alloy lead to the formation of the compounds Ag_3Sn, $Ag_{0.8}Sn_{0.2}$, $In_{0.2}Sn_{0.8}$ and AgZn. The addition of Bi and Zn at level 2 wt.% to the Sn–3.5Ag increases the dynamic Young's modulus, hardness, yield strength, delay the fracture strength and improves the creep resistance due to generate fine grain size in the Sn–Ag solder as a result of rapid solidification. The addition of In, Bi and Zn to the Sn–3.5Ag binary system lowers the melting temperature.

Acknowledgement

I express my deep gratitude and appreciation to Professor M. Kamal, Head of Metal Physics Group, Physics Department, Faculty of Science, Mansoura University, Mansoura, Egypt.

References

[1] S. Jin, JOM 45 (1993) 13.
[2] W.L. Winterbottom, JOM 45 (1993) 20.
[3] L.E. Felton, C.H. Raeder, D.B. Knorr, C.H. Havsy, Proc. 1992 Int. Electron. Manufact. Symp., vol. 300, 1992.
[4] C. Melton, Proc. 1993 IEEE Int. Symp. Electron. Environ., vol. 94, 1993.
[5] W.J. Tomlinson, A. Fullylove, J. Mater. Sci. 27 (1992) 5777.
[6] C. Melton, JOM 45 (1993) 33.
[7] V.I. Igshev, J.I. Kleiman, J. Electron. Mater. 2 (2000) 29.
[8] M. McCormack, S. Jin, G.W. Kammlott, H.S. Chen, Appl. Phys. Lett. 63 (15) (1993).
[9] M. Hirano, K. Suetsugu, A. Yamagushi, H. Kuwata, K. Uji, H. Takano, Proc. Fifth Symp. Microjoining Assembly Technol. Electron., Yokohama, Japan, 4–5 February, The Japan Welding Society, Japan, 1999, p. 393.
[10] C. Wei, Y.C. Liu, Y.J. Han, J.B. Wan, K. Yang, J. Alloys Compd. 464 (1–2) (2008) 301.
[11] Jingbo Wan, Yongchang Liu, Chen Wei, Zhiming Gao, J. Alloys Compd. 463 (1–2) (2008) 230.
[12] Jun Shen, Yongchang Liu, Yajing Han, Houxiu Gao, Rare Metals 25 (2006) 365.
[13] Jun Shen, Yong-Chang Liu, Ya-Jing Han, Hou-xiu Gao, Chen Wei, Yu-gin Yang, Trans. Nonferrous Met. Soc. China 59 (2006) 16.
[14] F. Gao, T. Takemoto, Mater. Lett. 60 (2006) 2315.
[15] Ikuo Shohji, Tomohiro Yoshida, Takehiko Takahashi, Susumu Hioki, Mater. Sci. Eng. A 50 (2004) 366.
[16] K. Narayan Prabhu, Rantej Bali, Rajat Ranjan, Mater. Des. 25 (2004) 447.
[17] B.D. Cullity, Elements of X-ray Diffraction, 2nd ed., Addison-Wesely Publishing Company, 1978, pp. 248.
[18] B.D. Cullity, Elements of X-ray Diffraction, 2nd ed., Addison-Wesely Publishing, USA, 1959, pp. 317 (Chapter 10).
[19] R.M. Shalaby, J. Alloys Compd. 480 (2009) 334.
[20] R.M. Shalaby, J. Mater. Electron. 16 (2005) 187.
[21] Mustafa Kamal, AbuBakr El-Bediwi, Tarek El-Ashram, J. Mater. Sci.: Mater. Electron. 15 (2004) 211.
[22] M. Kamal, E.S. Goda, Mater. Manuf. Proc. 21 (2006) 736.